Journal of Environmental Chemical Engineering 9 (2021) 105191

Contents lists available at ScienceDirect

Journal of Environmental Chemical Engineering

journal homepage: www.elsevier.com/locate/jece

High performance functionalized UiO metal organic frameworks for the efficient and selective adsorption of Pb (II) ions in concentrated multi-ion systems

George S. Morcos [a], Amr Awad Ibrahim [b,c], Mayyada M.H. El-Sayed [a,1,*], M. Samy El-Shall [b,2,*]

[a] Chemistry Department, American University in Cairo, AUC Avenue, New Cairo 11835, Egypt
[b] Department of Chemistry, Virginia Commonwealth University, Richmond, VA 23284, USA
[c] Chemistry Department, Faculty of Science, Mansoura University, Mansoura 35516, Egypt

ARTICLE INFO

Keywords:
UiO MOFs
Grafting
Adsorption
Lead
Water treatment

ABSTRACT

In this work, we report novel amine-functionalized zirconium-based metal organic frameworks (MOFs) for the efficient and selective removal of Pb (II) in concentrated multi-component heavy metal ions systems. Pristine UiO-66 and UiO-67 MOFs were grafted with thiourea and amidinothiourea via a facile one-step post synthetic modification. This is the first report on grafting of amidinothiourea onto MOFs. Successful grafting was confirmed by Fourier transform infrared spectroscopy, X-ray diffraction and X-ray photoelectron spectroscopy. A mechanism involving dehydration, ionization and coordination steps was proposed for grafting and subsequent Pb (II) binding. The microporous amidinothiourea modified UiO-66 and UiO-67 MOFs demonstrated excellent performance in their high maximum adsorption capacities of 246 and 367 mg.g^{-1}, respectively, as well as their remarkable selectivity for Pb (II) ions in highly concentrated multi-ion solutions. This is, in addition, to their effective removal efficiencies which reached up to more than 95% at a high range of Pb (II) concentrations (25–250 ppm). Furthermore, the structural stability of the MOF crystals was maintained after adsorption and the MOF was completely regenerated for up to four cycles. The developed MOFs can thus be utilized as reliable adsorbents for Pb (II) removal from industrial wastewater effluents.

1. Introduction

The increase in global industrial activities has led to the discharge of hazardous heavy metals that are either biologically toxic or carcinogenic into the natural water bodies [1]. Lead is a major water contaminant that has significant negative impacts on human health and the environment [2]. With regard to health, lead can cause central nervous system damage and deterioration in the brain function, in addition to failure in kidney, liver, and the reproductive system [3]. According to the Institute of Health Metrics and Evaluation of the US, lead exposure in 2015 accounted for about half a million of deaths and loss of about nine million lives among adults above 15 years of age [4]. Lead diffuses into natural water bodies through the discharge effluents of battery manufacturers, lead smelters, printing and mining industries, and it adversely affects the marine environment [5,6].

Adsorption is a promising technique for water treatment due to its potential efficiency, selectivity, and suitability for scaling up, in addition to the reusability of its adsorbents. It utilizes various inorganic adsorbent materials such as zeolites, activated carbon, activated silica, carbon nanotubes; or organic materials such as polymeric resins, or a hybrid of the two. However, these materials might suffer from low adsorption capacities due to their insufficient surface area, low selectivity or difficulty in regeneration [7,8]. The utilization of metal organic frameworks (MOFs) as adsorbent materials shows potential for overcoming these drawbacks since they offer highly porous structures with large internal surface areas which enhance their uptake capacity [9]. Their well-defined pores and channel structures which allow for tailorable guest-host interactions can potentially enhance their selectivity [8,10].

The interactions of MOFs with heavy metals can be tuned via their functionalization or modification, which is achieved by incorporating

* Corresponding authors.
E-mail addresses: Mayyada@aucegypt.edu (M.M.H. El-Sayed), mselshal@vcu.edu (M.S. El-Shall).
[1] 0000–0001-6257–5748
[2] 0000–0002-1013–4948

https://doi.org/10.1016/j.jece.2021.105191
Received 16 November 2020; Received in revised form 8 January 2021; Accepted 5 February 2021
Available online 10 February 2021

new functional groups into their structure. Although the modification can be performed prior to or during MOF synthesis, however, post synthetic modification (PSM) is recommended to avoid interference of the new functional groups with the formation of the MOF [11]. Modification of the MOF could be realized through non covalent interactions, coordinate interactions, covalent bonding, and metalation [12]. Coordinative interaction between a functional ligand and the metal center is known as "grafting", which essentially requires the removal of auxiliary ligands through dehydration of the MOF to generate coordinatively unsaturated sites (CUS) that can act as Lewis acid sites at the metal node of the MOF [13,14]. These sites have been successfully utilized for grafting several MOFs such as HKUST, which was grafted with pyridine [15], glycine [16], and dithioglycol [17] as new axial ligands; in addition to MIL-100-Fe which was grafted by polydopamine (PDA) [18], as well as MIL-100-Cr that was grafted with methanol [19]. Furthermore, MIL-101-Cr was grafted with ethylenediamine [13,20], ethanolamine [21], diethanolamine [21], diethylenetriamine (DETA) [22], tetraethylenepentamine (TEPA) [23], melamine [24], urea [24], and adenine [25].

One important class of MOFs is the zirconium-based MOFs, in which zirconium ion is bound to an organic linker such as terephthalate, biphenyldicarboxylate, and benzene tricarboxylate, to yield UiO-66 MOF, UiO-67 MOF and MOF-808, respectively [26–28]. Pure UiO-66 and UiO-67 MOFs involve 12-coordinate bonds between the Zr center and the other organic ligands, the highest coordination reported to date for a MOF. In comparison to other MOFs, Zr-based MOFs are characterized by high thermal stability, water stability, and chemical stability in acidic media [29], which arise due to the high bonding strength between the inorganic brick and the organic linker. The bond between the benzene ring and the terminal carboxyl group is the weakest in the structure, which implies that changing the ligand would not alter the stability of a Zr-based MOF [30]. In terms of their structures, UiO MOFs can exhibit defects in their crystalline structure, when missing one or more linkers, metal ions or nodes [31–34], thus introducing Zr CUSs as open sites for functionalization. Bronsted sites can also be formed by the water and hydroxyl groups coordinated to the Zr atoms [35,36]. Examples of grafted Zr-based MOFs are MOF-808 that was grafted through its formate auxiliary ligands by ethylene diaminetetraacetic acid (EDTA), oxalic acid (OX) and thioglycollic acid (TGA) [37], as well as UiO-66 that was modified by alkylamine [38] and ethylenediamine [39]. Pristine UiO-66 and UiO-67 exhibited high thermal stability, in which their chemical structures were sustained at high temperatures up to 520° C. It was also reported that UiO-66 and UiO-67 maintained their thermal stability after grafting with electron rich groups [25,38,39].

Several MOFs and their nanocomposites have been investigated as potential adsorbents for lead. One popular class of MOFs are the MILs such as MIL-101-ED [20], Al-MIL-53-NH_2/Fe_3O_4 [40], MIL-53-NH_2(M) [41], MIL-53-NH_2(W) [41], MIL-68(M) [41], MIL-68(W) [41], and MIL-100-PDA [18] which achieved maximum adsorption capacities of 88, 62.9, 159.5, 188.6, 136.8, 254.9, and 394.0 mg g^{-1}, respectively. As for the Zirconium-based MOFs such as DUT-67 [42], UiO-66-NH_2 [43], UiO-66-NHC(S)NHMe [44], and UiO-66-EDTA [45], they showed maximum adsorption capacities of 98.5, 166.7, 232.0, and 357.9 mg g^{-1}, respectively; whereas a higher adsorption capacity of 616.6 mg g^{-1} was reported for a zinc-based MOF [46]. However, these MOFs still suffered from issues such as sophisticated synthesis involving multi-step processes, low removal efficiencies particularly at high Pb (II) concentrations, low selectivity and difficulty in regeneration [47,48]. This work aims at developing novel functionalized MOFs that can efficiently and selectively remove lead ions in single and multi-component aqueous systems via adsorption. Thus, the synthesis will involve a facile one-step process where highly stable UiO-66 and UiO-67 MOFs will be grafted with thiourea and amidinothiourea to obtain UiO-66-thiourea, UiO-66-amidinothiourea, UiO-67-thiourea and UiO-67-amidinothiourea, which will henceforth be referred to as UiO-66-TU, UiO-66-AT, UiO-67-TU, and UiO-67-AT, respectively. This is the first report of amidinothiourea modified MOFs, however thiourea modified ones were studied for comparison purposes with regard to the adsorption capacity and binding mechanism. The study will entail characterization of the prepared pristine and functionalized MOFs using Fourier Transform Infrared (FTIR) spectroscopy, Brunauer Emmet and Teller (BET) analysis, X-ray Diffraction (XRD), and X-ray Photoelectron Spectroscopy (XPS), as well as studying their morphology using Scanning Electron Microscopy (SEM), then evaluating their performance in adsorbing Pb^{2+} from single and multi-component systems, and finally assessing their selectivity and regeneration capacity.

2. Materials and methods

2.1. Chemicals

All chemicals were of analytical grade, purchased from commercial sources and used without further purification. Zirconium chloride (>99%), terephthalic acid, TPA (>98%) and 4,4′-biphenyldicarboxylic acid, BPDC (97%) were obtained from Sigma Aldrich (USA), hydrochloric acid (38%), dimethylformamide, DMF (99%), anhydrous dimethylformamide, DMF (>99.8%), amidinothiourea (99%), thiourea (>99%), lead nitrate, mercury chloride, nickel chloride, cupric chloride, and zinc nitrate were obtained from Fluka (USA).

2.2. Preparation of adsorbents

2.2.1. Synthesis of pristine UiO-66 and UiO-67

UiO-66 and UiO-67 were synthesized according to previous literature under solvothermal conditions using HCl as a modulating agent [49]. Briefly, 625 mg of $ZrCl_4$ were dissolved with the organic linker in 75 mL DMF containing 5 mL HCl under sonication for 10 min. Masses of 615 mg TPA and 450 mg BPDC were used as organic linkers in UiO-66 and UiO-67, respectively. Then the solution was transferred to an autoclave and heated at 393 K for 24 h. After cooling to room temperature (298 K), the resultant white solid product was collected via centrifugation (Beckman Allegra 21 R) at 10,000 rpm for 10 min. The as-synthesized UiO-66 and UiO-67 were further purified by a two-step process to remove unreacted TPA or BPDC, by means of washing with DMF followed by ethanol (99%), for three times. Washing was conducted in an ultra-sonicator (VWR model 50T) for 10 min and was followed by centrifugation at 10,000 rpm for 10 min.

2.2.2. Grafting of UiO-66 and UiO-67

The prepared UiO-66 and UiO-67 MOFs were modified with thiourea or amidinothiourea via coordination bonding between the sulfur atom (–S-C) in thiourea or amidinothiourea and the CUSs generated from the defected Zr_6 clusters of the MOF after dehydration [2]. The procedure was adopted from previous literature with slight modification [20,24,39]. Typically, 0.1 g of the as-synthesized UiO-66 or UiO-67 was dehydrated and degassed at 523 K in a vacuum oven for 12 h to remove associated water molecules and thus generate CUSs, and then suspended in 50 mL of anhydrous DMF. Afterwards, thiourea or amidinothiourea was added in excess amount (0.2 g) and the mixture was refluxed for 12 h. The final product was collected by centrifugation, followed by washing with DMF and ethanol for three times, and then drying overnight in an oven at 333 K. A schematic diagram showing the steps of the MOFs' synthesis and modification is illustrated in Fig. 1.

2.2.3. Characterization of the MOFs

The crystalline nature of the as-synthesized and modified MOFs was investigated using the powder X-ray diffractometer B Ruker D8 system. All XRD patterns were displayed as diffractograms with 2-theta (2Θ) scan ranging from 3° to 50° and step increment of 0.01° per 1 s. FTIR spectroscopy was conducted using Thermo Scientific Nicolet 380 FTIR instrument. The samples were prepared as pellets by mixing and grinding 1 mg of MOF sample with 100 mg of analytical grade

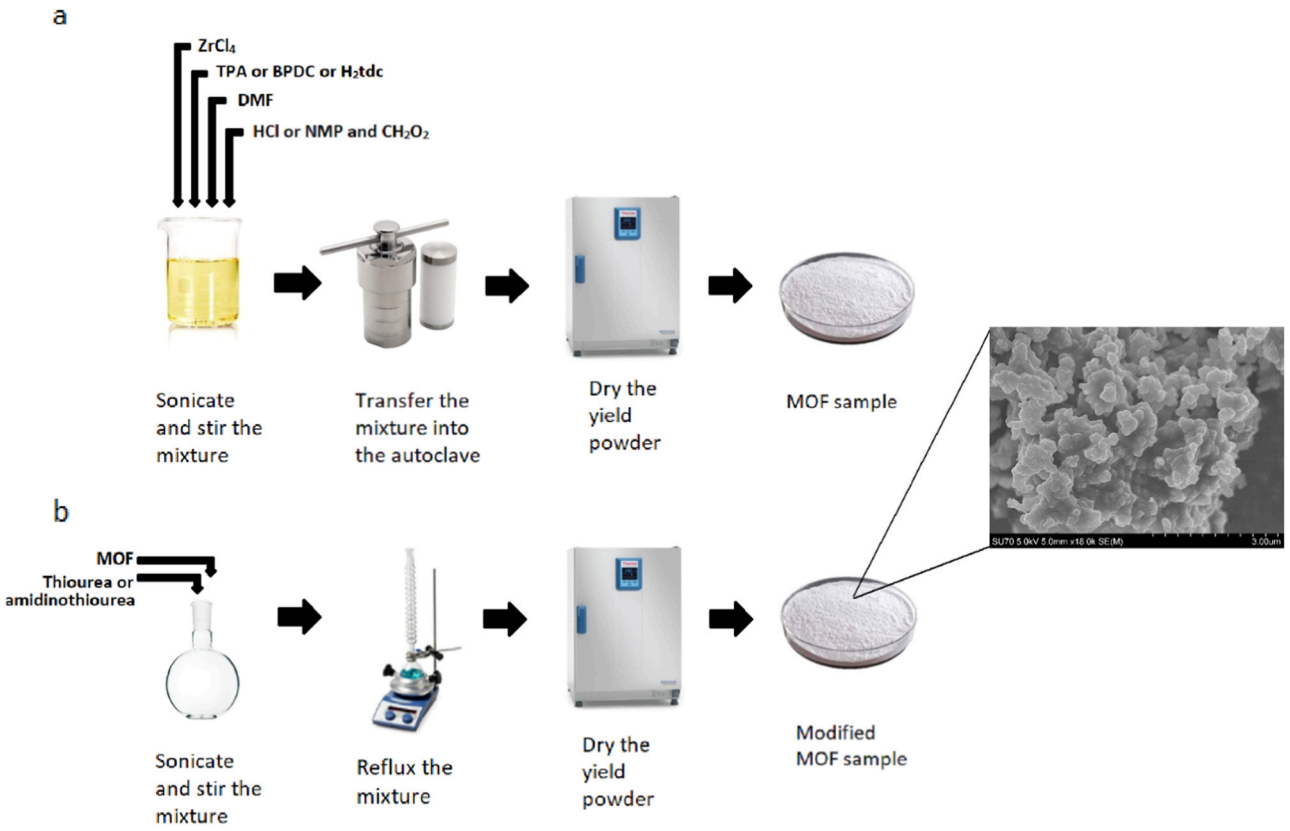

Fig. 1. Synthesis of (a) as-synthesized MOFs and (b) their modification.

potassium bromide (KBr) in a mortar. The mixture was then compressed with a hydraulic piston to form the pellet, and samples were scanned from 400 to 4000 cm^{-1} with an average recording of 32 scans. Textural properties of the different MOFs and their modified derivatives were determined using the Micrometrics ASAP 2020 instrument employing the BET method. A dry powdered sample of about 100 g was placed in the designated tube of ASAP 2020. The tube was mounted into the system and degassed below 50 μmHg at 100 °C for 8 h. Nitrogen gas was used to generate adsorption/desorption isotherms at −196 °C. BET and Langmuir surface areas were calculated, and the average pore volume was estimated using the Barret, Joyner, and Halenda (BJH) model.

Surface morphologies of the MOF samples were obtained using the HITACHI SU-70 SEM, with dual magnification power modes; low magnification mode (20x to 2000x) and high magnification mode (100x to 800,000x). Elemental composition of each MOF was analyzed by XPS using Thermo Fisher ESCALAB 250. Samples were scanned from 0 to 1400 eV, and their elemental spectra were further deconvoluted to analyze the bonding of individual species.

2.2.4. Adsorption equilibrium studies

Batch contacting sorption experiments were conducted in a series of vials. For equilibrium studies, stock solutions of $Pb(NO_3)_2$ were prepared in deionized water with initial concentrations (C_o) of 25, 50, 100, 250, 500 and 1000 mg L^{-1}. To each 10 mL of Pb (II) solution, 10 mg of adsorbent were added and the pH was adjusted by adding either 0.1 M HNO_3 or 0.1 M NaOH. The vials were then left to shake over a magnetic stirrer for 12 h at room temperature (23 ± 2 °C) and pH of 5.5 ± 0.2. This pH was chosen to avoid the protonation of the amine groups of the adsorbent at lower pHs, as well as the precipitation of Pb ions that occurs at higher pHs. The solution was then centrifuged at 10,000 rpm for 10 min, and the supernatant was then collected to be analyzed for Pb ion concentration using Inductively Coupled Plasma (ICP), Thermo Scientific ICP-AES 7400 and Agilent ICP-OES 5110. Experiments were carried out in triplicate and the Pb ion concentrations were calculated based on a constructed calibration curve.

To construct the equilibrium isotherm, the amount of Pb adsorbed at equilibrium was calculated according to the following equation [50].

$$q_e = \frac{C_0 V - C_e V}{m} \tag{1}$$

where q_e (mg.g^{-1}) is the equilibrium adsorption capacity, C_o (mg.L^{-1}) is the initial concentration of Pb (II) ions, C_e (mg.L^{-1}) is the equilibrium concentration of Pb (II) ions in solution, m (g) is the mass of adsorbent, and V (L) is the volume of Pb (II) solution.

The percentage removal (% removal) was calculated as follows: [50].

$$\%Removal = \frac{C_o - C_e}{C_o} \times 100 \tag{2}$$

Langmuir isotherm model was used to describe the monolayer adsorption of Pb (II) onto the MOF surface, the linear form of which is given by Eq. (3) [51].

$$\frac{C_e}{q_e} = \frac{C_e}{q_m} + \frac{1}{K_L q_m} \tag{3}$$

where, q_m represents the maximum (Langmuir) adsorption capacity (mg.g^{-1}), and K_L is the Langmuir constant. From the linear plot of C_e/q_e vs C_e, q_m and K_L can be determined from $1/q_m$ and $1/K_L q_m$ which represent the intercept and the slope, respectively.

Freundlich isotherm which assumes a heterogenous surface of active sites was also used to model the adsorption of Pb(II) onto the MOF surface, and its linear form is described by Eq. (4) [51].

$$\log q_e = \log K_f + \frac{1}{n} \log c_e \tag{4}$$

Where K_f and n are Freundlich constants.

Hill isotherm model was used to describe the cooperative binding of

different adsorbates onto a homogenous substrate. The linear form of this isotherm is given by Eq. (5) [52].

$$\log\frac{q_e}{q_m - q_e} = n_H \log C_e - \log K_D \quad (5)$$

Where n_H and K_D are Hill isotherm constants.

Temkin isotherm model was used to assess the influence of adsorbate – adsorbate interactions on the adsorption process. The linear form of the Temkin model is given by Eq. (6) [52].

$$q_e = \frac{RT}{b_T}\ln K_T + \frac{RT}{b_T}\ln C_e \quad (6)$$

Where K_T and b_T are Temkin isotherm constants.

2.2.5. Adsorption kinetic studies

Batch kinetic experiments were performed at an initial Pb (II) concentration of 25 mg L^{-1} using 50 mg of adsorbent dispersed in 50 mL solution placed in an Erlenmeyer flask. Samples were drawn at specific time intervals (5, 10, 15, 30, 45, 60, 120, 240 and 480 min), and the supernatants were separated by centrifugation. The experiments took place at room temperature (23 ± 2 °C) and pH of 5.5 ± 0.2.

The kinetic mechanism and the relevant rate constants were estimated by using the pseudo-first and pseudo-second order kinetic models. The pseudo-first order rate assumes a rate of reaction directly proportional to the number of unoccupied sites [53], as in Eq. (7) and its linearized form is given in Eq. (8) [54].

$$\frac{dq}{dt} = k_1(q_e - q) \quad (7)$$

$$\ln(q_e - q) = \ln q_e - k_1 t \quad (8)$$

where q_e (mg g^{-1}) is the amount of adsorbate taken up on the surface of the MOF adsorbent at equilibrium, while q (mg g^{-1}) is the adsorbate uptake at time t, and k_1 (min^{-1}) is the kinetic rate constant for the interaction between the adsorbate and the solid phase.

The pseudo-second order kinetic model assumes the rate of reaction to be directly proportional to the square of the number of unoccupied sites on the adsorbent surface as in Eq. (9). The integration of Eq. (9) would yield a linearized form of the equation as shown by Eq. (10) [51].

$$\frac{dq}{dt} = k_2 (q_e - q)^2 \quad (9)$$

$$\frac{t}{q} = \frac{1}{k_2 q_e^2} + \frac{t}{q_e} \quad (10)$$

Where k_2 (g mg^{-1} min^{-1}) [2] is the rate constant for the pseudo-second order reaction.

The mechanism underlying adsorption was tested using Morris and Weber intraparticle diffusion (IPD) model as in Eq. (11) [54].

$$q = k_{id} t^{0.5} + c \quad (11)$$

Where k_{id} is the rate constant for intra-particle diffusion and c is a constant related to external diffusion.

2.2.6. Selectivity tests

The selectivity of UiO-66-AT toward Pb (II) ions was evaluated by conducting adsorption in the presence of various competitive metal ions. A mixture of Pb (II), Hg (II), Cu (II), Ni (II) and Zn (II) ions was prepared by dissolving 250 mg L^{-1} of each metal ion in deionized water. A volume of 10 mL of this solution was left to shake with 10 mg of the adsorbent for 6 h, after which the solutions were centrifuged and the concentrations of Pb (II), Hg (II), Cu (II), Ni (II) and Zn (II) ions in the supernatants were measured by ICP.

2.2.7. Regeneration studies

The regeneration studies were carried out at Pb(II) concentration of 25 ppm. An amount of 50 mg of each of UiO-66-AT and UiO-67-AT was added to 50 mL of $Pb(NO_3)_2$ solution in an Erlenmeyer flask, and left to shake for 2 h. The MOF was then dried overnight at 80 °C and subsequently treated with a 0.1 M solution of ethylene diaminetetraacetic acid (EDTA) for 2 h. Then, it was washed with water and dried overnight at 80 °C. The process was repeated for four cycles.

2.2.8. Statistical analysis

All measurements were conducted in triplicate and expressed as mean± SD. Statistical analyses were performed to test the significance of results using the two-tailed student's *t*-test at a 95% level of confidence, while linear regression analysis was performed on Origin-lab software, version 9.6.5.169, to predict the equilibrium and kinetic models.

3. Results and discussion

3.1. Structural and morphological properties

The XRD patterns of UiO-66, UiO-66-TU, and UiO-66-AT, as well as those of UiO-67, UiO-67-TU, and UiO-67-AT are shown in Fig. 2a and b, respectively. The crystal structures of UiO-66 and UiO-67 were confirmed by the characteristic peaks obtained at 7.5°, 8.6°, and 12.2° for UiO-66, and at 5.4° and 6.7° for UiO-67, as in agreement with previous literature [30,49,55,56]. Upon grafting each of UiO-66 and UiO-67 with either thiourea or amidinothiourea, the XRD patterns remained unchanged as evident from Fig. 2a and b, respectively, indicating that the crystal structures of both MOFs remained intact after grafting.

Fig. 2c depicts the XRD patterns after the adsorption of Pb (II) ions onto both UiO-66 functionalized MOFs. Adsorption resulted in the appearance of three new peaks illustrated by arrows in Fig. 2c at 23.43°, 26.78°, and 27.72°; along with an increase in the intensities of the peaks that range between 20 and 30°. The changes associated with the guest molecule adsorption can be attributed to the generation of new $Pb_3(CO_3)_2(OH)_2$ crystals which could have been formed upon dehydration of the MOF [57]. A similar conclusion can be inferred for UiO-67 functionalized MOFs.

FTIR spectroscopy was used to determine the main functional groups pertaining to the as-synthesized MOFs and their modified derivatives. Fig. 3a shows the FTIR spectra of UiO-66, UiO-66-TU, and UiO-66-AT, where the two functionalized MOFs exhibit peaks at 1060 cm^{-1} that can be attributed to C–N symmetric stretching [20]. In addition, UiO-66-AT shows peaks at 3370 and 3185 cm^{-1} that can be assigned to the stretching of the amine groups [58]. The FTIR spectra of UiO-67, UiO-67-TU, and UiO-67-AT are depicted in Fig. 3b, where UiO-67-TU and UiO-67-AT show the same peaks pertaining to –NH and C–N stretching at the same respective wavenumbers as their UiO-66 modified derivatives.

To investigate the surface morphology and the microstructure of the MOFs and their functionalized derivatives, they were characterized by SEM as shown in Figs. S1(a-f). Defective pristine UiO-66 particles possess a nearly spherical structure that was maintained after modification with thiourea and amidinothiourea as shown in Figs. S1a, S1b and S1c, respectively; while UiO-67 and its UiO-67-TU and UiO-67-AT derivatives display irregular rounded shapes with a wide size distribution as shown in Figs. S1d, S1e and S1f, respectively. The irregular shape may provide a larger surface area for adsorption as compared to the spherical

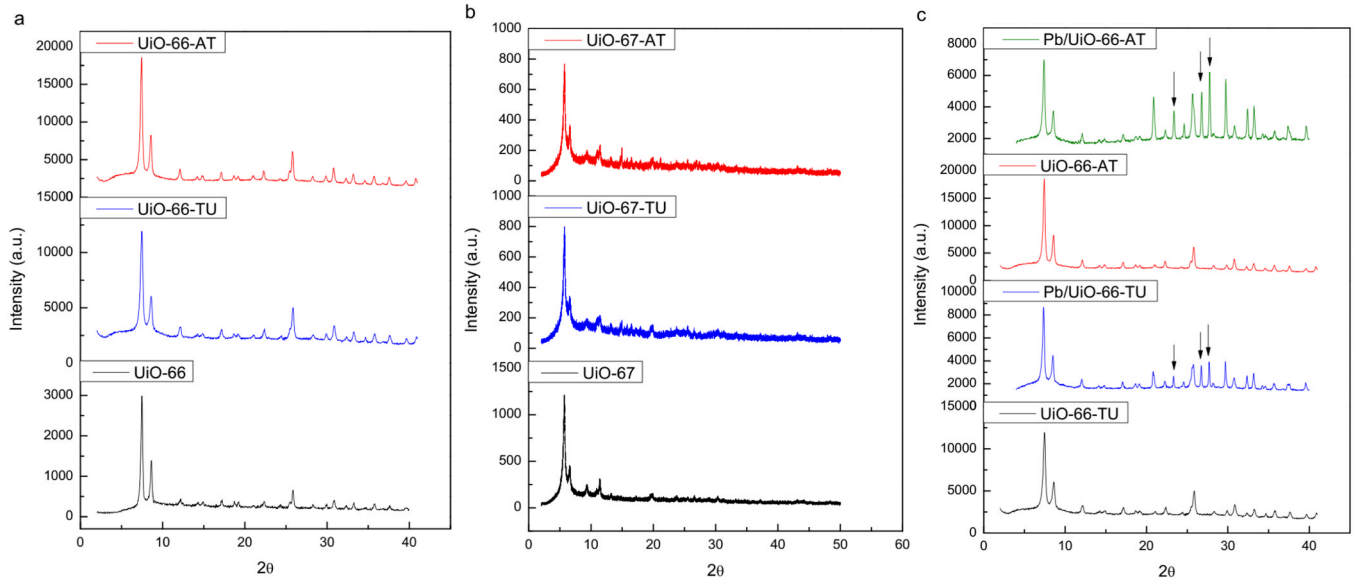

Fig. 2. XRD patterns of (a) as-synthesized UiO-66 MOF (black, bottom), UiO-66-TU (blue, middle), and UiO-66-AT (red, top), (b) as-synthesized UiO-67 MOF (black, bottom), UiO-67-TU (blue, middle), and UiO-67-AT (red, top), (c) UiO-66-TU and UiO-66-AT before and after Pb adsorption (For interpretation of the references to color in this figure legend, the reader is referred to the web version of this article).

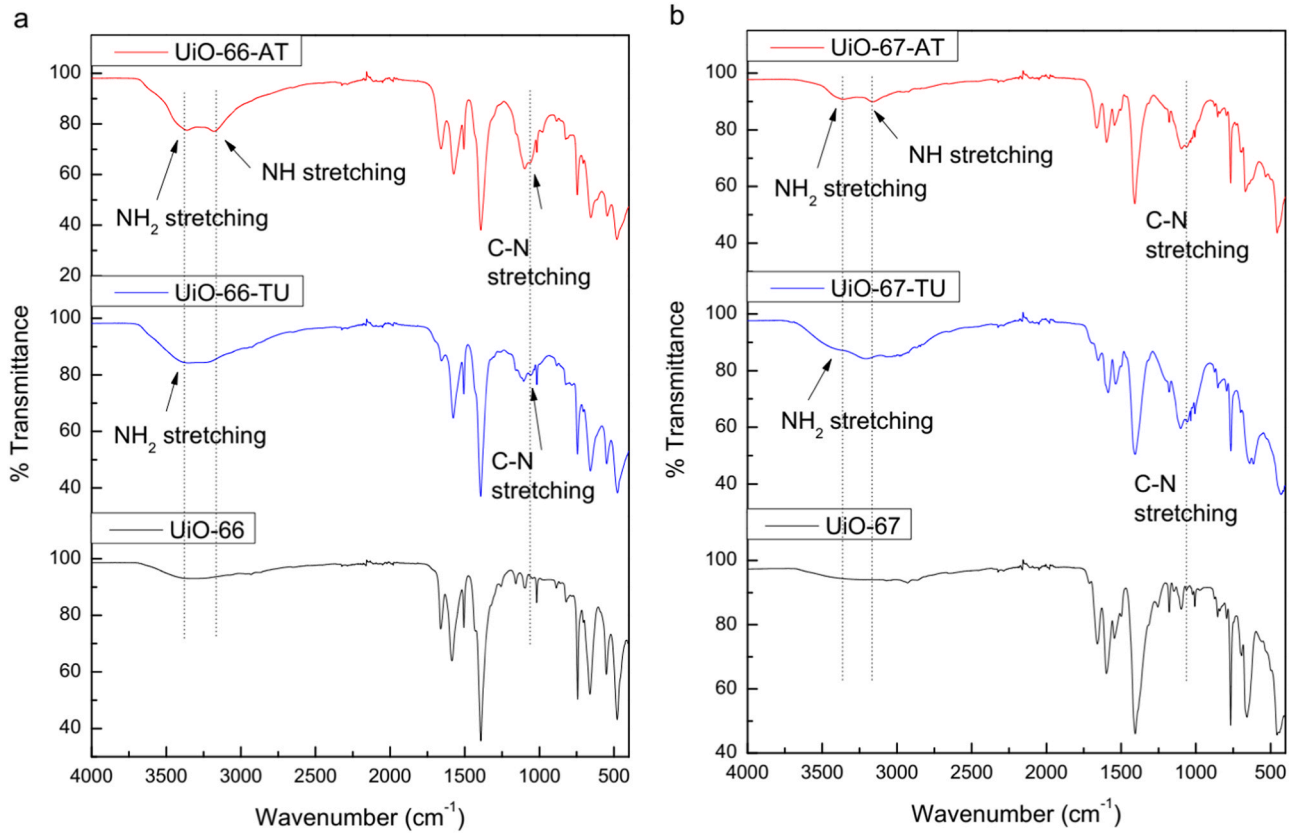

Fig. 3. FTIR spectra of (a) as-synthesized UiO-66 MOF (black, bottom), UiO-66-TU (blue, middle), and UiO-66-AT (red, top), (b) as-synthesized UiO-67 MOF (black, bottom), UiO-67-TU (blue, middle), and UiO-67-AT (red, top) (For interpretation of the references to color in this figure legend, the reader is referred to the web version of this article).

shape. The SEM images of the as-synthesized UiO-66 and UiO-67 MOFs match those in literature where HCl was used as a modulator [59]. Further, the SEM images of the MOFs prior and post modification depict similar morphologies. As previously indicated by XRD, the MOFs also maintained their crystalline structure after modification. These findings together could imply that the MOFs maintained their stability after modification with the organic moieties. From experimental observations, the synthesized MOFs were stable in water at pH 5.5 for up to 12 h.

3.2. Adsorption capacity as a performance indicator

Prior to constructing the adsorption isotherms for the different employed MOFs, adsorption was conducted under different pHs in order to determine the optimum pH range for further equilibrium and kinetic studies. In fact, pH affects the adsorption capacity of metal ions in aqueous solutions as a result of the protonation and deprotonation of the functional groups attached on the adsorbent's surface [53]. The effect of pH on the equilibrium adsorption capacity (q_e) of UiO-66-TU and UiO-66-AT for Pb (II) is depicted in Fig. S2, where q_e increases with increasing the pH. This could be attributed to the deprotonation of the amino groups which act as chelating binding sites for Pb ions. At pH 5, the adsorption capacities start to equilibrate and approach their maximum values. Thus, the pH range from 5.5 to 6 will be employed in further studies in order to exploit the maximum adsorption for Pb (II) ions, and in the meantime, avoid any possible precipitation of Pb (II) ions at the higher pH ranges.

The isotherms pertaining to the adsorption of Pb (II) onto UiO-66 and its modified derivatives (UiO-66-TU and UiO-66-AT) at pH 5.5 ± 0.2 are shown in Fig. 4a, while those of UiO-67 and its modified derivatives (UiO-67-TU and UiO-67-AT) are shown in Fig. 4b.

Clearly, all the isotherms show hyperbolic curves indicative of a Langmuirian-type relationship with monolayer coverage. In addition, isotherms of the modified MOFs of UiO-66 and UiO-67 exhibit higher adsorption capacities relative to their pristine counterparts. By linearizing these isotherms and fitting them to the linear form of the Langmuir model equation, the maximum adsorption capacities (q_m) of UiO-66, UiO-66-TU and UiO-66-AT were estimated to be 48.7 ± 8.6, 206.6 ± 4.3, and 245.8 ± 1.7 mg g^{-1}, respectively, with R^2 values of 0.9511, 0.9984 and 0.9999, confirming the goodness of this fit (Fig. S3). This indicates that UiO-66-AT exhibited the highest adsorption capacity for Pb ions which amounts to about 5 times higher than that of the pristine UiO-66. Similarly, the adsorption capacities of UiO-67, UiO-67-TU and UiO-67-AT were determined as 55.8 ± 2.4, 252.3 ± 4.3 and 366.6 ± 2.8 mg g^{-1}, respectively, with R^2 values of 0.9920, 0.9994 and 0.9998 (Fig. S4). Accordingly, UiO-67-AT showed the highest capacity which is 6.5 times higher than that of its pristine form and 1.5 times higher than its UiO-66 counterpart. The isotherms were also fitted to the Freundlich model and the linear forms are shown in Figs. S5 and S6, however, lower correlation factors were obtained as compared to the Langmuir fits. The UiO-67-AT isotherms were also fitted to the Temkin and Hill isotherms as shown respectively in Figs. S7 and S8, however, lower correlation factors were obtained relative to the Langmuir fits.

In view of the above, MOFs functionalized with amidinothiourea yielded the highest lead adsorption capacities compared to the pristine and thiourea-modified MOFs. Therefore, further studies will focus on UiO-66-AT and UiO-67-AT.

3.3. Textural properties and XPS analysis

BET analysis was conducted to determine the surface area and pore volume of the UiO-66-AT and UiO-67-AT as well as their pristine forms. For all the investigated MOFs, the N_2 adsorption-desorption isotherms revealed a typical microporous material with the majority of pores less than 2 nm, as shown in Figs. S9 (a-c). The BET and Langmuir surface areas along with the pore volumes of the pristine MOFs and their derivatives are listed in Table 1. Clearly, UiO-66-AT possesses comparable surface areas and pore volume to that of pristine UiO-66. However, its adsorption capacity is much higher than that of UiO-66 due to its functionality. On the other hand, the Langmuir and BET surface areas of UiO-67 as well as its pore volume declined by about 50% upon modification to UiO-67-AT. The decrease in the surface area and pore volume of UiO-67 after modification can be ascribed to the partial blockage of the pores by the amidinothiourea moieties that probably diffused into the crystal structure of UiO-67 MOF [20]; but however failed to diffuse into the pores of UiO-66 which have been reported to be smaller than those of UiO-67 [60]. Despite that, UiO-67-AT possesses slightly higher BET and Langmuir surface areas than that of UiO-66-AT which could explain its slightly higher Pb (II) adsorption capacity relative to UiO-66-AT. This is consistent with the SEM morphology study discussed earlier.

XPS was used to investigate the elemental composition of the employed MOFs before and after Pb adsorption. Fig. 5a and b show the survey XPS spectra of UiO-66, UiO-66-AT, UiO-66-AT-Pb, UiO-67, UiO-67-AT and UiO-67-AT-Pb. According to these spectra, UiO-66 and UiO-67 are similarly composed of Zr, O, C with slightly different percentage

Table 1
Surface areas and pore volumes of UiO MOFs and their amidinothiourea derivatives.

MOF	BET S.A. (m^2g^{-1})	Langmuir S.A. (m^2g^{-1})	Pore volume (cm^3)
UiO-66	846.8	1239.1	0.347
UiO-66-AT	886.5	1295.2	0.369
UiO-67	2011.4	2599.3	0.651
UiO-67-AT	920.39	1411.6	0.329

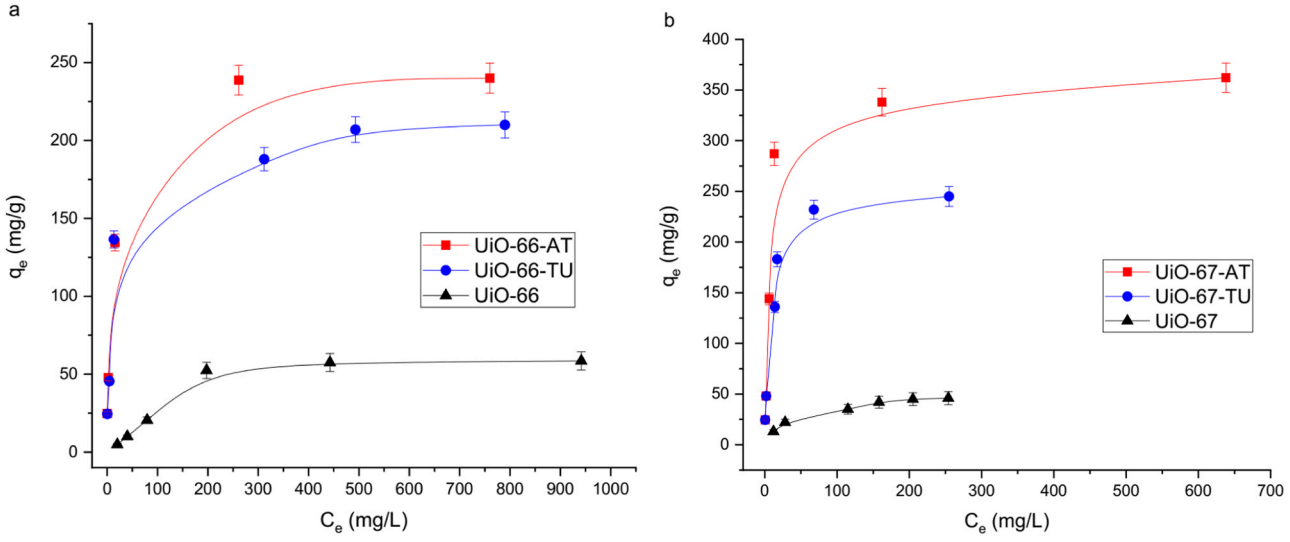

Fig. 4. Adsorption isotherm of (a) UiO-66 along with its modified derivatives, and (b) UiO-67 along with its modified derivatives at pH 5.5 ± 0.2 and 23 ± 2 °C. Values shown are mean ± SD (n = 3).

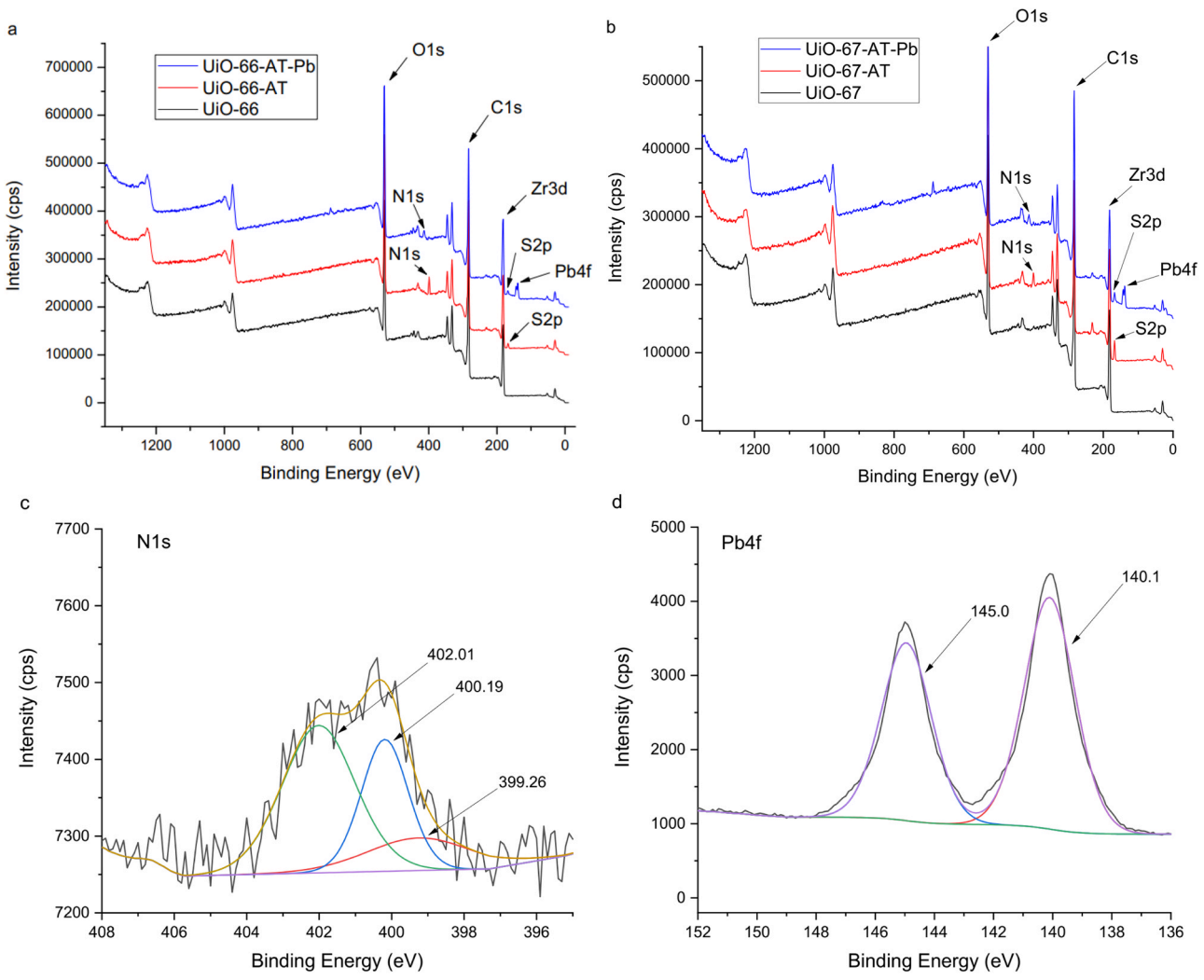

Fig. 5. XPS spectra for (a) survey of UiO-66 and its derivatives, (b) survey of UiO-67 and its derivatives, (c) N1s of UiO-67-AT-Pb, and (d) Pb 4 f of UiO-67-AT-Pb.

compositions, as reported in previous literature [61,62]. The deconvoluted XPS spectra of the O1s, C1s, and Zr3d elemental components are shown in Fig. S10 and the elemental composition of UiO-67-AT is presented in Table S1. In addition, UiO-66-AT and UiO-67-AT possess the N and S elements as evident from their respective binding energies at 398.9 and 167.8 eV, and this confirms the successful grafting of

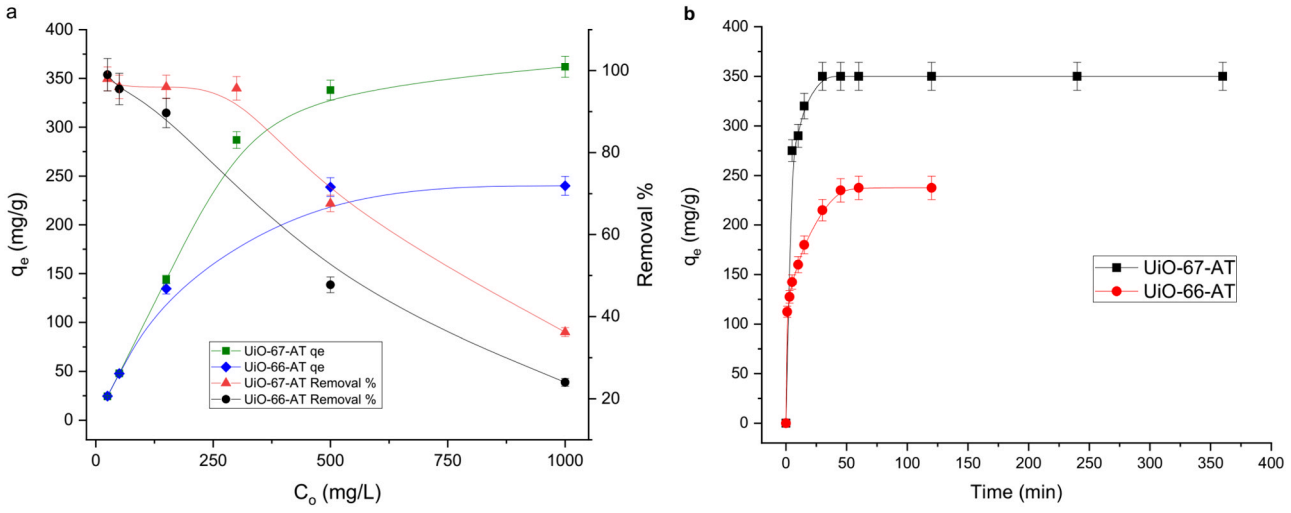

Fig. 6. Effect of (a) initial concentration, and (b) time on Pb (II) adsorption onto UiO-66-AT and UiO-67-AT at pH 5.5 ± 0.2 and 23 ± 2 °C. Values shown are mean ± SD ($n = 3$).

amidinothiourea [50]. Furthermore, the Pb peak appears at 170 eV for both UiO-66-AT-Pb and UiO-67-AT-Pb, which confirms the presence and successful binding of Pb species to the modified MOF framework. By comparing the survey spectrum of UiO-67-AT to its UiO-67-AT-Pb counterpart, a shift to a higher binding energy can be observed for N1s. This finding along with the accompanied change in N1s atomic composition (Table S2) after Pb was adsorbed could indicate that Pb was bound to nitrogen-containing groups. Fig. 5c represents the N1s binding energy spectrum of UiO-67-AT-Pb deconvoluted into three peaks at 398.8, 400.19, and 402.04 eV which may correspond to C=N, R_2NH, and NH_2, respectively. Similar findings were previously reported [18,63]. Fig. 5d shows the deconvoluted Pb 4 f binding energy spectrum of UiO-67-AT-Pb, in which the energy peaks at 144.73 and 139.92 eV correspond to Pb^{2+} oxidation state and pertain to Pb 4 $f_{5/2}$ and Pb 4 $f_{7/2}$, respectively [20]. Similar behavior was observed for UiO-66-AT and its UiO-66-AT-Pb counterpart.

3.4. Investigation of the operating parameters

The adsorption capacities of UiO-66-AT and UiO-67-AT were investigated using different initial concentrations of Pb solutions, while controlling other variables such as temperature at 23 ± 2 °C, pH 5.5 ± 0.2, adsorbent dosage of 1 g/L, and contact time of 12 h. The relevant adsorption profiles are depicted in Fig. 6a, where a direct proportionality between the adsorption capacity and the initial lead concentration can be observed for both adsorbents. As the initial concentration increases, a larger concentration gradient is formed leading to enhanced mass transport and higher adsorption capacity. At the highest employed initial concentrations, the adsorption capacity is not affected by increasing the concentration due to saturation of the binding sites. The higher adsorption capacity of UiO-67-AT relative to UiO-66-AT could be attributed to its larger BET surface area and pore size which allowed for more exposure of binding sites as discussed earlier [60]. Fig. 6a also shows the percent removal of Pb (II) ions using UiO-66-AT and UiO-67-AT, where the removal clearly declines with increasing the initial concentration again as a result of saturation of active sites [51,54]. UiO-67-AT and UiO-66-AT showed maximum percent removal of 36% and 24%, respectively, at an initial Pb (II) concentration of 1000 ppm. Much higher removal efficiencies (>95%) were attained at initial concentrations below 250 ppm. Fig.6b illustrates the effect of contact time on the adsorption of Pb (II) onto UiO-66-AT and UiO-67-AT at pH 5.5 ± 0.2, using an adsorbent dose of 1 g/L and an initial concentration of 1000 ppm. In addition to its higher adsorption capacity relative to UiO-66-AT, UiO-67-AT showed faster adsorption of Pb^{2+} ions where it reached complete saturation after 30 min as opposed to 50 min for UiO-66-AT. This could also be ascribed to the larger pores of UiO-67-AT relative to UiO-66-AT as alluded to earlier [60].

3.5. Adsorption kinetics

The kinetic profiles for lead adsorption by UiO-67-AT at an initial Pb (II) concentration of 1000 ppm are depicted as linear plots pertaining to the pseudo-first order (Figs. S11) and pseudo-second order (Fig. S12) kinetic models. The adsorption is better described by the pseudo-second order kinetic model as confirmed by the higher correlation factor (R^2) [53]. This implies that adsorption is governed by both surface reaction and diffusion mechanisms. The pseudo-first order (k_1) and pseudo-second order (k_2) rate constants were obtained from the slopes and the intercepts of the linear plots and their estimated values are given in Table S3, in addition to their corresponding R^2 values.

To further investigate the adsorption mechanism of Pb(II) ions onto UiO-67-AT, the intraparticle diffusion model was applied and its linear plot is depicted in Fig. S13, in which the intercept suggests that adsorption is not solely governed by pore diffusion, but is also driven by boundary layer diffusion [64].

3.6. Comparison with other MOFs

The maximum adsorption capacities of lead by UiO-66-AT and UiO-67-AT were compared to those of other MOF adsorbents previously reported in literature, as presented in Table 2. Among the MOFs developed in this study, UiO-67-AT exhibits the highest maximum adsorption capacity of 366.6 ± 2.8, exceeding that of UiO-66-AT by 1.5 times. Furthermore, UiO-67-AT maximum adsorption capacity is higher than most of those reported in literature, except for the two MOFs MIL-100-PDA and Zn_3L_3(BPE). For MIL-100-PDA, the adsorption capacity is comparable to that of UiO-67-AT exceeding it inappreciably with only 7%. In addition, the synthesis of UiO-67-AT employed a more facile single-step process in which the as-synthesized functional molecules were grafted onto the MOF's framework as opposed to a two-step process reported for the other two MOFs. Besides, UiO-67-AT, unlike the other two MOFs, provides excellent removal efficiencies (> 95%) for a high range of Pb (II) concentrations (25–250 ppm). Zn_3L_3(BPE), for example, exhibits this removal efficiency within a lower range of concentrations (10–75 ppm), after which it substantially declines. MIL-100-PDA, as well, works for low concentrations since it was mainly designed for treatment of drinking water. UiO-67-AT, however, would be highly efficient for industrial wastewater treatment.

3.7. Adsorption selectivity

To investigate the selectivity of UiO-66-AT and UiO-67-AT MOFs for Pb (II) adsorption in multi-component systems, Zn (II), Ni (II), Cu (II), and Hg (II) ions were chosen as competitor ions due to their being divalent as Pb (II). The adsorption capacities of UiO-66-AT and UiO-67-AT for Pb (II) and the co-existing ions in a multi-component system of initial concentration of 250 ppm for each metal ion are shown in Fig. 7a. Both UiO-66-AT and UiO-67-AT MOFs were most selective for Pb (II) ions with respective adsorption capacities of 128.5 ± 6.4 and 207.5 ± 10.4, followed by Hg (II) ions with capacities of 49.0 ± 2.5 and 35.0 ± 2.8. This can be explained in view of the ionic radii of Pb (II), Zn (II), Ni (II), Cu (II), and Hg (II) which are 0.118, 0.075, 0.069, 0.073 and 0.102 nm, respectively.

The high selectivity towards Pb (II) ions exhibited by both MOFs can be attributed to the larger ionic radius and lower molar Gibbs energy of hydration of Pb ions compared to other ionic species, which facilitated their coordination with the grafted amino-terminated species [46,66].

3.8. Regeneration

In order to test for the reusability of the developed MOFs, the regeneration capacities of UiO-66-AT and UiO-67-AT were determined

Table 2
Maximum lead adsorption capacities reported for different MOFs.

MOF/MOF nanocomposite	q_m, mg. g^{-1}	pH	Temperature,° C	Reference
Cu(tpa)/GO	37	7	25	[65]
UiO-66	48.7	5–5.5	23 ± 2	This study
UiO-67	55.8	5–5.5	23 ± 2	This study
Al-MIL-53-NH2/Fe3O4	62.9	6	25	[40]
Cr-MIL-101-ED	88.0	6	25	[20]
DUT-67	98.5	5–5.5	25	[42]
MIL-68(M)	136.8	6	–	[41]
MIL-53-NH_2(M)	159.5	6	–	[41]
UiO-66-NH_2	166.7			[43]
MIL-53-NH_2(W)	188.6	6	–	[41]
UiO-66-NHC(S)NHMe	232.0	–	–	[44]
UiO-66-AT	245.8	5–5.5	23 ± 2	This study
MIL-68(W)	254.9	6	–	[41]
UiO-66-EDTA	357.9	7	30	[45]
UiO-67-AT	366.6	5–5.5	23 ± 2	This study
MIL-100-PDA	394.0	7	28	[18]
[$Zn_3L_3(BPE)_{1.5}$].4.5DMF	616.6	6	25	[46]

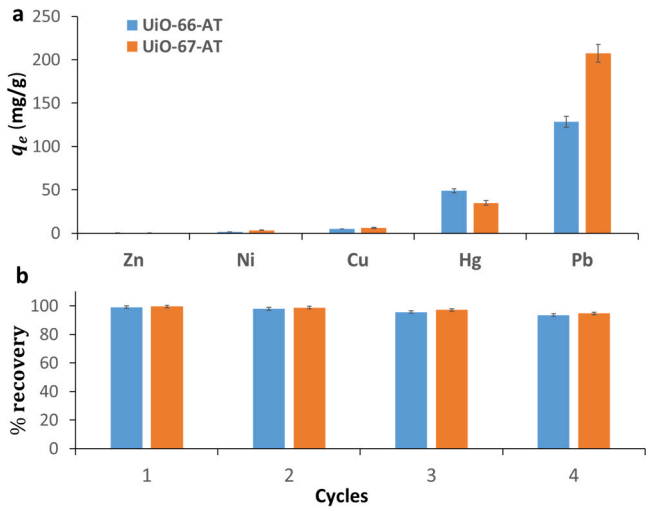

Fig. 7. (a) Adsorption capacities of UiO-66-AT and UiO-67-AT for Pb (II) adsorption in a multicomponent system using 250 ppm Pb (II) at pH 5.5 ± 0.2, and (b) their % recovery after regeneration for four consecutive cycles. Values shown are mean ± SD ($n = 3$).

using EDTA-2Na as a desorbent. First, adsorption was conducted using 25 ppm of Pb (II) solution at pH 5.5 ± 0.2. In each regeneration cycle, 50 mg samples of Pb/UiO-66-AT and Pb/UiO-67-AT complexes were treated with 100 mL of a 0.05 M EDTA solution under stirring for 2 h at 298 K. This process was repeated such that the MOF complexes were regenerated in four successive adsorption-desorption cycles, and their adsorption capacities were determined for each cycle as depicted in Fig. 7b. The results show that the MOFs can be successfully regenerated for four cycles with no significant decrease, according to student's *t*-test, in % recovery which increased the 99%. Following the desorption process, Pb ions can be recovered by solvent extraction using strong acids to strip the metal off the chelate, then the metal can be concentrated in a subsequent step [67].

3.9. Mechanism of binding and interaction

To investigate the binding of thiourea and amidinothiourea onto UiO-67, the FTIR spectra of thiourea and amidinothiourea were compared to the spectra of UiO-67-TU and UiO-67-AT, respectively. As shown in Fig. 8a, the peak at 1470 cm^{-1} in the thiourea spectrum which can be assigned to the N-C-N stretching vibration, has been shifted to 1500 cm^{-1} in the UiO-67-AT spectrum. This shift can be attributed to the increase in the double bond character of the carbon to nitrogen bond

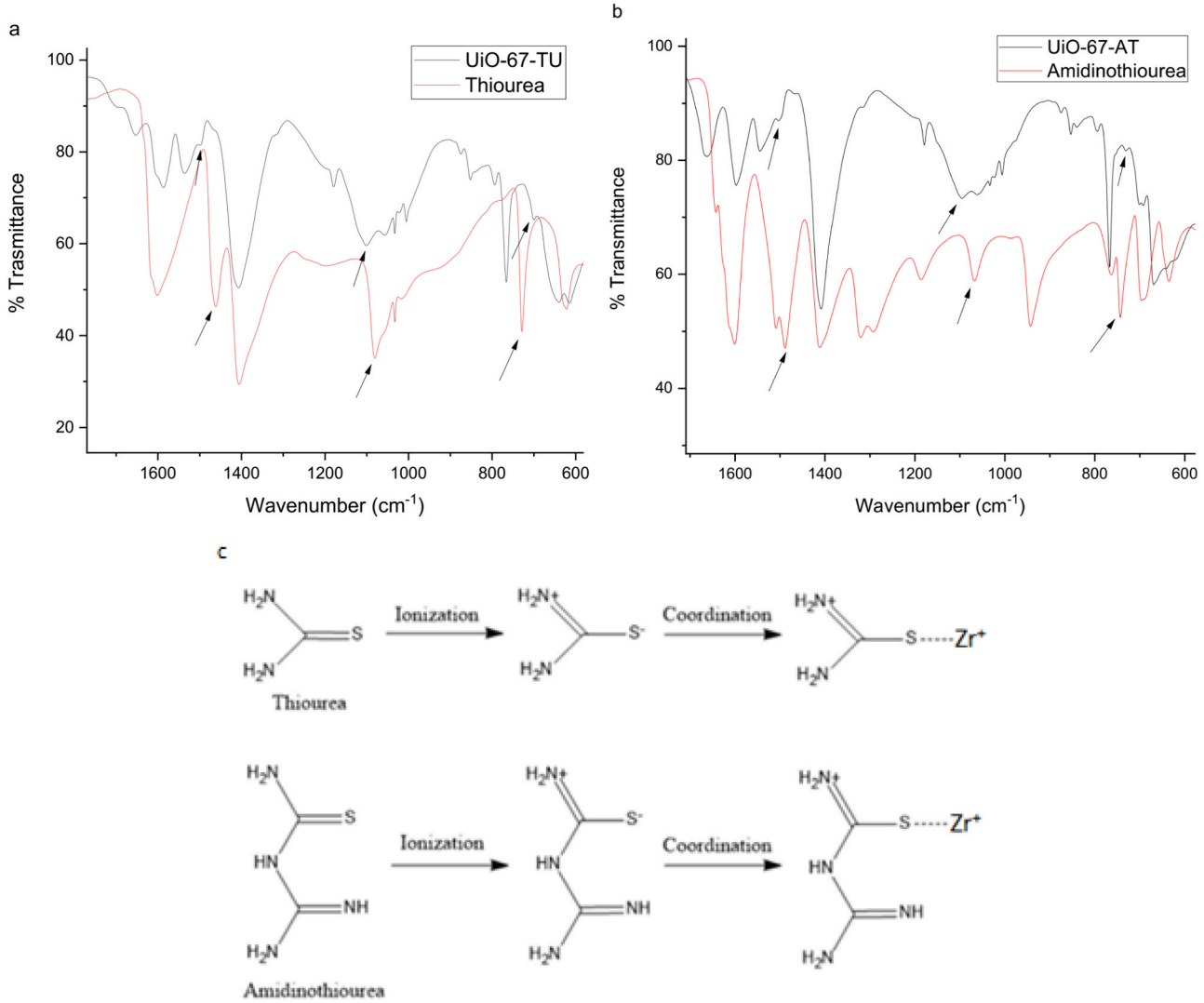

Fig. 8. FTIR spectra of (a) thiourea and UiO-67-TU, (b) amidinothiourea and UiO-67-AT, (c) possible mechanism for the ionization of thiourea and amidinothiourea followed by their coordination with the Zr center [58].

associated with complex formation. Moreover, as shown in Fig. 8a, the peak observed at 730 cm^{-1} in the thiourea spectrum was shifted to about 700 cm^{-1} in the complex spectrum of UiO-67-TU, probably due to the decrease in the double bond character of the C=S bond of the thiourea molecule [58,68].

Moreover, a noticeable difference between the spectrum of thiourea and that of the thiourea modified MOF, UiO-67-TU, appears in the region at about 1100 cm^{-1}, where a strong absorption band in the thiourea spectrum appears at 1081 cm^{-1} but then weakens and shifts to 1100 cm^{-1} in the spectrum of UiO-67-TU probably due to change in the nature of the C=S bond upon coordination. These results confirm the successful grafting of UiO-67 with thiourea. The shifting of these bands is similar to those reported in literature, where thiourea was investigated for its coordination with transition metals [58].

The modification of the UiO-67 MOF showed similar changes in the FTIR bands of UiO-67-AT MOF with respect to the amidinothiourea molecule (Fig. 8b). This similarity in behavior entails the coordination of the amidinothiourea to the metal center of the MOF possibly through the sulfur atom and this was probably accompanied by a change in the double bond nature from C=S to C-S as evident from the red shift in the 740 cm^{-1} band of the amidinothiourea spectrum. Accordingly, the amidinothiourea molecule was concluded to exhibit a similar form of coordination as that of the thiourea molecule. In view of the above findings, an interaction mechanism can be proposed as depicted in Fig. 8c, which displays the ionization and coordination of thiourea and amidinothiourea molecules with the zirconium metal ion.

Fig. 9 depicts the proposed molecular mechanism for the grafting of the MOF and its subsequent binding to the Pb (II) ions. First, the MOF is activated through the dehydration and unsaturation of the metal centers. The ionized functional organic species subsequently coordinates to the unsaturated metal ion in the metal cluster of the MOF as previously proposed in Fig. 8c. The electron rich thiourea and amidinothiourea groups could be favorable for the MOF's stability as it was previously reported that electron rich amine groups enhanced the stability of UiO-66 [39]. Finally, the free Pb (II) metal ions bind and chelate to the functional nitrogen-containing moieties of thiourea or amidinothiourea through coordination bonding as depicted in Fig. 9b and c, respectively. XPS results, pseudo-second order kinetics, along with monolayer adsorption onto microporous materials suggest the chemisorption of Pb ions onto the MOF.

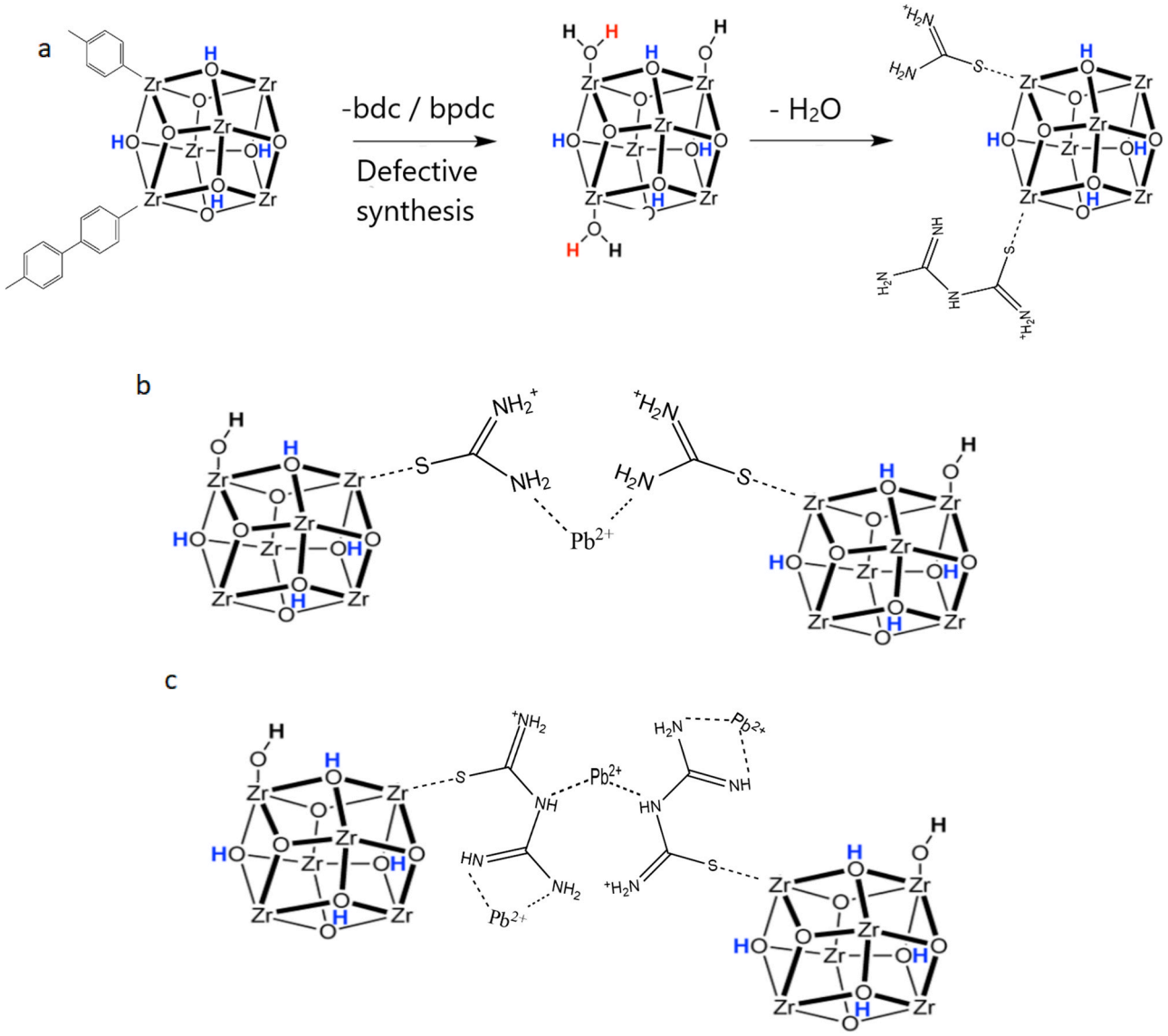

Fig. 9. (a) Generation of CUS in UiO-based MOFs and grafting with thiourea or amidinothiourea, (b) binding of Pb^{2+} ions to the thiourea grafted MOF, (c) binding of Pb^{2+} ions to the amidinothiourea grafted MOF.

4. Conclusion

In this work, novel modified Zr-based MOFs were developed by grafting defected pristine UiO-66 and UiO-67 MOFs with thiourea and amidinothiourea in a facile one-step post synthetic modification process. Successful grafting was confirmed with XRD, FTIR and XPS, while the microporous structure of the MOF was determined by BET. A mechanism was proposed for the grafting of the MOF via dehydration and unsaturation of its metal centers followed by ionization and coordination of thiourea and amidinothiourea with the Zr metal ions. Amidinothiourea modified UiO-66 and UiO-67 effectively removed Pb (II) ions from aqueous solutions with respective maximum adsorption capacities of 245.8 ± 1.7 and 366.6 ± 2.8 mg g^{-1}, which account for about 5 and 6.5 times higher than their pristine counterparts. They, as well, exhibited excellent removal efficiencies ($> 95\%$) for a high range of Pb (II) concentrations (25–250 ppm). XRD confirmed the structural stability of the MOF crystals after the modification and adsorption processes, while XPS suggested that lead binding occurred via coordination bonding with the nitrogen-containing moieties of the MOF. Furthermore, the synthesized MOFs showed high selectivity for lead ions in heavily concentrated multi-component systems containing other heavy metal ions. They were also efficiently regenerated for up to four cycles while maintaining their original adsorption capacity. The high performance of the developed MOFs renders them reliable adsorbents for treating industrial wastewater effluents.

Supporting information

SEM, effect of pH on Pb adsorption, Langmuir, Freundlich, Temkin, Hill and BET isotherms, XPS deconvoluted spectra, elemental composition, atomic nitrogen percentage, Pseudo first and second order kinetics, and intraparticle diffusion model.

Author Contributions

The manuscript was written through contributions of all authors. All authors have given approval to the final version of the manuscript. All authors contributed equally.

CRediT authorship contribution statement

Mayyada El-Sayed: Conceptualization, Methodology, Software. **Samy El-Shall**: Conceptualization, Methodology, Software. **George Morcos**: Conceptualization, Methodology, Software. **Amr Ibrahim:** Conceptualization, Methodology, Software. **George Morcos**: Data curation, Writing - original draft preparation. **Amr Ibrahim:** Data curation, Writing - original draft preparation. **George Morcos**: Visualization, Investigation. **Mayyada El-Sayed**: Visualization, Investigation. **Samy El-Shall**: Supervision. **Mayyada El-Sayed:** Supervision. **George Morcos**: Software, Validation. **Amr Ibrahim:** Software, Validation. **George Morcos**: Writing - review & editing. **Mayyada El-Sayed:** Writing - review & editing.

Declaration of Competing Interest

The authors declare no conflict of interest.

Acknowledgments

The authors would like to thank Virginia Commonwealth University, VA, US and The American University in Cairo, Egypt for funding this project. We also thank the National Science Foundation (CHE-1900094) for the support of this work. MSE acknowledges support from the Mary E. Kapp Endowed Chair fund.

Appendix A. Supporting information

Supplementary data associated with this article can be found in the online version at doi:10.1016/j.jece.2021.105191.

References

[1] P.N. Obasi, B.B. Akudinobi, Potential health risk and levels of heavy metals in water resources of lead–zinc mining communities of Abakaliki, Southeast Nigeria, Appl. Water Sci. 10 (7) (2020), 184, https://doi.org/10.1007/s13201-020-01233-z.
[2] L. Aljerf, M. Aljurf Improvements in the Ecological and Nutritional Aspects of Down's Syndrome. Preprints 2020, 2020050512. https://doi.org/10.21203/rs.3.rs-30313/v1.
[3] J. Goel, K. Kadirvelu, C. Rajagopal, V. Kumar Garg, Removal of lead(ii) by adsorption using treated granular activated carbon: batch and column studies, J. Hazard. Mater. 125 (1) (2005) 211–220, https://doi.org/10.1016/j.jhazmat.2005.05.032.
[4] Heavy Metals | Environmental Performance Indexhttps://epi.envirocenter.yale.edu/2018-epi-report/heavy-metals (Accessed May 10, 2020).
[5] M. Khajeh, Z.S. Heidari, E. Sanchooli, Synthesis, characterization and removal of lead from water samples using lead-ion imprinted polymer, Chem. Eng. J. 166 (3) (2011) 1158–1163, https://doi.org/10.1016/j.cej.2010.12.018.
[6] K. Kordas, J. Ravenscroft, Y. Cao, E.V. McLean, Lead exposure in low and middle-income countries: perspectives and lessons on patterns, injustices, economics, and politics, IJERPH 15 (11) (2018) 2351, https://doi.org/10.3390/ijerph15112351.
[7] F. Fu, Q. Wang, Removal of heavy metal ions from wastewaters: a review, J. Environ. Manag. 92 (3) (2011) 407–418, https://doi.org/10.1016/j.jenvman.2010.11.011.
[8] J.-R. Li, J. Sculley, H.-C. Zhou, Metal–organic frameworks for separations, Chem. Rev. 112 (2) (2012) 869–932, https://doi.org/10.1021/cr200190s.
[9] J. Wang, Y. Wang, H. Hu, Q. Yang, J. Cai, From metal–organic frameworks to porous carbon materials: recent progress and prospects from energy and environmental perspectives, Nanoscale 12 (7) (2020) 4238–4268, https://doi.org/10.1039/C9NR09697C.
[10] H. Xue, Q. Chen, F. Jiang, D. Yuan, G. Lv, L. Liang, L. Liu, M. Hong, A regenerative metal-organic framework for reversible uptake of Cd(Ii): from effective adsorption to in situ detection, Chem. Sci. 7 (9) (2016) 5983–5988, https://doi.org/10.1039/C6SC00972G.
[11] M. Kalaj, S.M. Cohen, Postsynthetic modification: an enabling technology for the advancement of metal-organic frameworks, ACS Cent. Sci. 6 (2020) 1046–1057, https://doi.org/10.1021/acscentsci.0c00690.
[12] Z. Wang, S.M. Cohen, Postsynthetic modification of metal-organic frameworks, Chem. Soc. Rev. 38 (5) (2009) 1315–1329, https://doi.org/10.1039/B802258P.
[13] Y.K. Hwang, D.-Y. Hong, J.-S. Chang, S.H. Jhung, Y.-K. Seo, J. Kim, A. Vimont, M. Daturi, C. Serre, G. Férey, Amine grafting on coordinatively unsaturated metal centers of MOFs: consequences for catalysis and metal encapsulation, Angew. Chem. Int. Ed. 47 (22) (2008) 4144–4148, https://doi.org/10.1002/anie.200705998.
[14] K.K. Tanabe, S.M. Cohen, Postsynthetic modification of metal–organic frameworks - a progress report, Chem. Soc. Rev. 40 (2) (2011) 498–519, https://doi.org/10.1039/C0CS00031K.
[15] S.S.-Y. Chui, S.M.-F. Lo, J.P.H. Charmant, A.G. Orpen, I.D. Williams, A chemically functionalizable nanoporous material [Cu3(TMA)2(H2O)3]n, Science 283 (5405) (1999) 1148–1150, https://doi.org/10.1126/science.283.5405.1148.
[16] N. Al-Janabi, H. Deng, J. Borges, X. Liu, A. Garforth, F.R. Siperstein, X. Fan, A facile post-synthetic modification method to improve hydrothermal stability and CO_2 selectivity of CuBTC metal–organic framework, Ind. Eng. Chem. Res. 55 (29) (2016) 7941–7949, https://doi.org/10.1021/acs.iecr.5b04217.
[17] F. Ke, L.-G. Qiu, Y.-P. Yuan, F.-M. Peng, X. Jiang, A.-J. Xie, Y.-H. Shen, J.-F. Zhu, Thiol-functionalization of metal-organic framework by a facile coordination-based postsynthetic strategy and enhanced removal of Hg2+ from water, J. Hazard. Mater. 196 (2011) 36–43, https://doi.org/10.1016/j.jhazmat.2011.08.069.
[18] D.T. Sun, L. Peng, W.S. Reeder, S.M. Moosavi, D. Tiana, D.K. Britt, E. Oveisi, W. L. Queen, Rapid, selective heavy metal removal from water by a metal-organic framework/polydopamine composite, ACS Cent. Sci. 4 (3) (2018) 349–356, https://doi.org/10.1021/acscentsci.7b00605.
[19] A. Vimont, J.-M. Goupil, J.-C. Lavalley, M. Daturi, S. Surblé, C. Serre, F. Millange, G. Férey, N. Audebrand, Investigation of acid sites in a zeotypic giant pores chromium(III) carboxylate, J. Am. Chem. Soc. 128 (10) (2006) 3218–3227, https://doi.org/10.1021/ja056906s.
[20] X. Luo, L. Ding, J. Luo, Adsorptive removal of Pb(II) Ions from aqueous samples with amino-functionalization of metal-organic frameworks MIL-101(Cr), J. Chem. Eng. Data 60 (6) (2015) 1732–1743, https://doi.org/10.1021/je501115m.
[21] P.W. Seo, B.N. Bhadra, I. Ahmed, N.A. Khan, S.H. Jhung, Adsorptive removal of pharmaceuticals and personal care products from water with functionalized metal-organic frameworks: remarkable adsorbents with hydrogen-bonding abilities, Sci. Rep. 6 (1) (2016), 34462, https://doi.org/10.1038/srep34462.
[22] S.-N. Kim, S.-T. Yang, J. Kim, J.-E. Park, W.-S. Ahn, Post-Synthesis functionalization of MIL-101 using diethylenetriamine: a study on adsorption and catalysis, CrystEngComm 14 (12) (2012) 4142–4147, https://doi.org/10.1039/C2CE06608D.

[23] X. Wang, H. Li, X.-J. Hou, Amine-functionalized metal organic framework as a highly selective adsorbent for CO_2 over CO, J. Phys. Chem. C 116 (37) (2012) 19814–19821, https://doi.org/10.1021/jp3052938.

[24] P.W. Seo, N.A. Khan, Z. Hasan, S.H. Jhung, Adsorptive removal of artificial sweeteners from water using metal–organic frameworks functionalized with urea or melamine, ACS Appl. Mater. Interfaces 8 (43) (2016) 29799–29807, https://doi.org/10.1021/acsami.6b11115.

[25] M. Sarker, J.Y. Song, A.R. Jeong, K.S. Min, S.H. Jhung, Adsorptive removal of indole and quinoline from model fuel using adenine-grafted metal-organic frameworks, J. Hazard. Mater. 344 (2018) 593–601, https://doi.org/10.1016/j.jhazmat.2017.10.041.

[26] R.J. Marshall, R.S. Forgan, Postsynthetic modification of zirconium metal-organic frameworks, Eur. J. Inorg. Chem. 2016 (27) (2016) 4310–4331, https://doi.org/10.1002/ejic.201600394.

[27] C.F. Pereira, A.J. Howarth, N.A. Vermeulen, F.A.A. Paz, J.P.C. Tomé, J.T. Hupp, O. K. Farha, Towards hydroxamic acid linked zirconium metal-organic frameworks, Mater. Chem. Front. 1 (6) (2017) 1194–1199, https://doi.org/10.1039/C6QM00364H.

[28] Z.-J. Lin, H.-Q. Zheng, Y.-N. Zeng, Y.-L. Wang, J. Chen, G.-J. Cao, J.-F. Gu, B. Chen, Effective and selective adsorption of organoarsenic acids from water over a Zr-based metal-organic framework, Chem. Eng. J. 378 (2019), 122196, https://doi.org/10.1016/j.cej.2019.122196.

[29] A.J. Howarth, Y. Liu, P. Li, Z. Li, T.C. Wang, J.T. Hupp, O.K. Farha, Chemical, thermal and mechanical stabilities of metal-organic frameworks, Nat. Rev. Mater. 1 (3) (2016), 15018, https://doi.org/10.1038/natrevmats.2015.18.

[30] J.H. Cavka, S. Jakobsen, U. Olsbye, N. Guillou, C. Lamberti, S. Bordiga, K. P. Lillerud, A new zirconium inorganic building brick forming metal organic frameworks with exceptional stability, J. Am. Chem. Soc. 130 (42) (2008) 13850–13851, https://doi.org/10.1021/ja8057953.

[31] D.M. Driscoll, D. Troya, P.M. Usov, A.J. Maynes, A.J. Morris, J.R. Morris, Characterization of undercoordinated Zr defect sites in UiO-66 with vibrational spectroscopy of adsorbed CO, J. Phys. Chem. C 122 (26) (2018) 14582–14589, https://doi.org/10.1021/acs.jpcc.8b03283.

[32] C. Caratelli, J. Hajek, F.G. Cirujano, M. Waroquier, i Llabrés, F.X. Xamena, V. Van Speybroeck, Nature of active sites on UiO-66 and beneficial influence of water in the catalysis of fischer esterification, J. Catal. 352 (2017) 401–414, https://doi.org/10.1016/j.jcat.2017.06.014.

[33] G.C. Shearer, S. Chavan, S. Bordiga, S. Svelle, U. Olsbye, K.P. Lillerud, Defect engineering: tuning the porosity and composition of the metal-organic framework UiO-66 via Modulated Synthesis, Chem. Mater. 28 (11) (2016) 3749–3761, https://doi.org/10.1021/acs.chemmater.6b00602.

[34] H. Wu, Y.S. Chua, V. Krungleviciute, M. Tyagi, P. Chen, T. Yildirim, W. Zhou, Unusual and highly tunable missing-linker defects in zirconium metal-organic framework UiO-66 and their important effects on gas adsorption, J. Am. Chem. Soc. 135 (28) (2013) 10525–10532, https://doi.org/10.1021/ja404514r.

[35] F. Vermoortele, B. Bueken, G. Le Bars, B. Van de Voorde, M. Vandichel, K. Houthoofd, A. Vimont, M. Daturi, M. Waroquier, V. Van Speybroeck, C. Kirschhock, D.E. De Vos, Synthesis modulation as a tool to increase the catalytic activity of metal-organic frameworks: the unique case of UiO-66(Zr), J. Am. Chem. Soc. 135 (31) (2013) 11465–11468, https://doi.org/10.1021/ja405078u.

[36] J. Canivet, M. Vandichel, D. Farrusseng, Origin of highly active metal–organic framework catalysts: defects? defects!, Dalton Trans. 45 (10) (2016) 4090–4099, https://doi.org/10.1039/C5DT03522H.

[37] Y. Peng, H. Huang, Y. Zhang, C. Kang, S. Chen, L. Song, D. Liu, C. Zhong, A versatile MOF-based trap for heavy metal ion capture and dispersion, Nat. Commun. 9 (1) (2018), 187, https://doi.org/10.1038/s41467-017-02600-2.

[38] L.-J. Li, P.-Q. Liao, C.-T. He, Y.-S. Wei, H.-L. Zhou, J.-M. Lin, X.-Y. Li, J.-P. Zhang, Grafting alkylamine in UiO-66 by charge-assisted coordination bonds for carbon dioxide capture from high-humidity flue gas, J. Mater. Chem. A 3 (43) (2015) 21849–21855, https://doi.org/10.1039/C5TA05997F.

[39] N. Erfaninia, R. Tayebee, M. Dusek, M.M. Amini, Ethylene diamine grafted nanoporous UiO-66 as an efficient basic catalyst in the multi-component synthesis of 2-aminithiophenes, Appl. Organo Chem. 32 (5) (2018), e4307, https://doi.org/10.1002/aoc.4307.

[40] F. Zhao, N. Song, W. Ning, Q. Jia, [Synthesis of magnetic metal organic framework Fe3O4@NH2-MIL-53 (Al) materials and application to the adsorption of lead], Guang Pu Xue Yu Guang Pu Fen. Xi Guang Pu 35 (9) (2015) 2439–2443.

[41] C.W. Abney, J.C. Gilhula, K. Lu, W. Lin, Metal-organic framework templated inorganic sorbents for rapid and efficient extraction of heavy metals, Adv. Mater. 26 (47) (2014) 7993–7997, https://doi.org/10.1002/adma.201403428.

[42] A.R. Geisse, C.M. Ngule, D.T. Genna, Removal of lead ions from water using thiophene-functionalized metal–organic frameworks, Chem. Commun. 56 (2) (2019) 237–240, https://doi.org/10.1039/C9CC09022C.

[43] N. Yin, K. Wang, Z. Li, Rapid microwave-promoted synthesis of Zr-MOFs: an efficient adsorbent for Pb(II) removal, Chem. Lett. 45 (6) (2016) 625–627, https://doi.org/10.1246/cl.160148.

[44] H. Saleem, U. Rafique, R.P. Davies, Investigations on post-synthetically modified UiO-66-NH2 for the adsorptive removal of heavy metal ions from aqueous solution, Microporous Mesoporous Mater. 221 (2016) 238–244, https://doi.org/10.1016/j.micromeso.2015.09.043.

[45] J. Wu, J. Zhou, S. Zhang, A. Alsaedi, T. Hayat, J. Li, Y. Song, Efficient removal of metal contaminants by EDTA modified mof from aqueous solutions, J. Colloid Interface Sci. 555 (2019) 403–412, https://doi.org/10.1016/j.jcis.2019.07.108.

[46] C. Yu, Z. Shao, H. Hou, A functionalized metal-organic framework decorated with O-groups showing excellent performance for lead(II) removal from aqueous solution, Chem. Sci. 8 (11) (2017) 7611–7619, https://doi.org/10.1039/C7SC03308G.

[47] J.E. Efome, D. Rana, T. Matsuura, C.Q. Lan, Metal-organic frameworks supported on nanofibers to remove heavy metals, J. Mater. Chem. A 6 (10) (2018) 4550–4555, https://doi.org/10.1039/C7TA10428F.

[48] P.A. Kobielska, A.J. Howarth, O.K. Farha, S. Nayak, Metal-organic frameworks for heavy metal removal from water, Coord. Chem. Rev. 358 (2018) 92–107, https://doi.org/10.1016/j.ccr.2017.12.010.

[49] M. J. Katz, Z. J. Brown, Y. J. Colón, P. W. Siu, K. A. Scheidt, R. Q. Snurr, J. T. Hupp, O. K. Farha, A facile synthesis of UiO-66, UiO-67 and their derivatives, Chem. Commun. 49 (82) (2013) 9449–9451, https://doi.org/10.1039/C3CC46105J.

[50] F. Awad, K.M. AbouZeid, W.M.A. El-Maaty, A.M. El-Wakil, M.S. El-Shall, Efficient removal of heavy metals from polluted water with high selectivity for Mercury(II) by 2-Imino-4-thiobiuret partially reduced graphene oxide (IT-PRGO), ACS Appl. Mater. Interfaces 9 (2017) 34230–34242, https://doi.org/10.1021/acsami.7b10021.

[51] O.S. Bayomie, H. Kandeel, T. Shoeib, H. Yang, N. Youssef, M.M.H. El-Sayed, Novel approach for effective removal of methylene blue dye from water using fava bean peel waste, Sci. Rep. 10 (1) (2020), 7824, https://doi.org/10.1038/s41598-020-64727-5.

[52] K.Y. Foo, B.H. Hameed, Insights into the modeling of adsorption isotherm systems, Chem. Eng. J. 156 (1) (2010) 2–10, https://doi.org/10.1016/j.cej.2009.09.013.

[53] L. Aljerf, High-efficiency extraction of bromocresol purple dye and heavy metals as chromium from industrial effluent by adsorption onto a modified surface of zeolite: kinetics and equilibrium study, J. Environ. Manag. 225 (2018) 120–132, https://doi.org/10.1016/j.jenvman.2018.07.048.

[54] S.G. Mohammad, M.M.H. El-Sayed, Removal of imidacloprid pesticide using nanoporous activated carbons produced via pyrolysis of peach stone agricultural wastes, Chem. Eng. Commun. 0 (0) (2020) 1–12, https://doi.org/10.1080/00986445.2020.1743695.

[55] X. Zhu, B. Li, J. Yang, Y. Li, W. Zhao, J. Shi, J. Gu, Effective adsorption and enhanced removal of organophosphorus pesticides from aqueous solution by Zr-based MOFs of UiO-67, ACS Appl. Mater. Interfaces 7 (1) (2015) 223–231, https://doi.org/10.1021/am5059074.

[56] Q. Yang, Y. Wang, J. Wang, F. Liu, N. Hu, H. Pei, W. Yang, Z. Li, Y. Suo, J. Wang, High effective adsorption/removal of illegal food dyes from contaminated aqueous solution by Zr-MOFs (UiO-67), Food Chem. 254 (2018) 241–248, https://doi.org/10.1016/j.foodchem.2018.02.011.

[57] L. Lv, N. Chen, C. Feng, J. Zhang, M. Li, Heavy metal ions removal from aqueous solution by xanthate-modified cross-linked magnetic chitosan/poly(Vinyl Alcohol) particles, RSC Adv. 7 (45) (2017) 27992–28000, https://doi.org/10.1039/C7RA02810E.

[58] A. Yamaguchi, R.B. Penland, S. Mizushima, T.J. Lane, C. Curran, J.V. Quagliano, Infrared absorption spectra of inorganic coördination complexes. XIV. infrared studies of some metal thiourea complexes1a, J. Am. Chem. Soc. 80 (3) (1958) 527–529, https://doi.org/10.1021/ja01536a005.

[59] K.A. Mocniak, I. Kubajewska, D.E.M. Spillane, G.R. Williams, R.E. Morris, Incorporation of cisplatin into the metal-organic frameworks UiO66-NH2 and UiO66 - encapsulation vs. conjugation, RSC Adv. 5 (102) (2015) 83648–83656, https://doi.org/10.1039/C5RA14011K.

[60] G.W. Peterson, S.-Y. Moon, G.W. Wagner, M.G. Hall, J.B. DeCoste, J.T. Hupp, O. K. Farha, Tailoring the pore size and functionality of UiO-type metal–organic frameworks for optimal nerve agent destruction, Inorg. Chem. 54 (20) (2015) 9684–9686, https://doi.org/10.1021/acs.inorgchem.5b01867.

[61] A. Wang, Y. Zhou, Z. Wang, M. Chen, L. Sun, X. Liu, Titanium incorporated with UiO-66(Zr)-type metal-organic framework (MOF) for photocatalytic application, RSC Adv. 6 (5) (2016) 3671–3679, https://doi.org/10.1039/C5RA24135A.

[62] L. Chen, X. Chen, H. Liu, C. Bai, Y. Li, One-step encapsulation of Pd nanoparticles in MOFs via a temperature control program, J. Mater. Chem. A 3 (29) (2015) 15259–15264, https://doi.org/10.1039/C5TA02860D.

[63] H. Zhu, J. Yuan, X. Tan, W. Zhang, M. Fang, X. Wang, Efficient removal of Pb2+ by Tb-MOFs: identifying the adsorption mechanism through experimental and theoretical investigations, Environ. Sci. Nano 6 (1) (2019) 261–272, https://doi.org/10.1039/C8EN01066H.

[64] A.A. Inyinbor, F.A. Adekola, G.A. Olatunji, Kinetics, isotherms and thermodynamic modeling of liquid phase adsorption of rhodamine B dye onto Raphia hookerie fruit epicarp, Water Resour. Ind. 15 (2016) 14–27, https://doi.org/10.1016/j.wri.2016.06.001.

[65] E. Rahimi, N. Mohaghegh, New hybrid nanocomposite of copper terephthalate mof-graphene oxide: synthesis, characterization and application as adsorbents for toxic metal ion removal from sungun acid mine drainage, Environ. Sci. Pollut. Res. 24 (28) (2017) 22353–22360, https://doi.org/10.1007/s11356-017-9823-6.

[66] Y. Marcus, Thermodynamics of solvation of ions. Part 5. - gibbs free energy of hydration at 298.15 K, J. Chem. Soc. Faraday Trans. 87 (18) (1991) 2995–2999, https://doi.org/10.1039/FT9918702995.

[67] K. Asemave, Greener chelators for recovery of metals and other applications, Org. Med. Chem. Int. J. 6 (4) (2018), https://doi.org/10.19080/OMCIJ.2018.06.555694.

[68] P.A. Ajibade, N.H. Zulu, A.O. Oyedeji, Synthesis, characterization, and antibacterial studies of some metal complexes of dialkyl thiourea: the X-ray single crystal structure of [CoCl2(Detu)2], Synth. React. Inorg. Met. Org. Nano Met. Chem. 43 (5) (2013) 524–531, https://doi.org/10.1080/15533174.2012.741179.